Silicon (2018) 10:1315–1327
https://doi.org/10.1007/s12633-017-9607-0

ORIGINAL PAPER

Abrasive Wear Characteristics of Silicon Carbide Particle Reinforced Zinc Based Composite

Mohammad Mohsin Khan[1] · **Gajendra Dixit**[1]

Received: 27 January 2016 / Accepted: 24 July 2017 / Published online: 23 October 2017

Abstract Herein, abrasive wear characteristics of SiCp dispersed zinc-aluminum based composites have been analyzed under high-stress condition. The wear tests were conducted on a Pin-on-Disc machine at a constant linear velocity of 1.57 m/s in the applied load range of 1-7 N while the abrasive platform used is 600 grit emery paper. A matrix alloy was also characterized under identical conditions to assess the influence of the dispersoid (SiC) particle on the wear behaviour. Wear rate, frictional heating and friction coefficient are the focused parameters of the study. The base alloy used has a dendrite structure comprising of α-dendrites surrounded by an $\alpha + \eta$ eutectoid and metastable ε phase in interdendritic regions. The composite shows similar features to those of the base alloy except the additional presence of the reinforcing SiC particles. The wear rate and friction coefficient decrease with increase in abrading distance while a reverse trend was observed in the case of frictional heating which gradually increases with the increase in abrading distance. Incorporation of SiC particles improves the wear resistance of the matrix alloy and increasing the percentage of SiC increases the frictional heating and reduces the friction coefficient of the test material. The wear mechanism has been understood through SEM examination of wear surface, subsurface, debris particles and degraded abrasive grit papers.

✉ Mohammad Mohsin Khan
mmohsinkhan511@gmail.com

[1] Department of Mechanical Engineering, Maulana Azad National Institute of Technology, Bhopal, India

Keywords Abrasive wear · Zinc-aluminium alloy · Metal matrix composite

1 Introduction

Due to the increase in the demand for light, rigid and strong material, metal matrix composites (MMC) have attracted the attention of many researchers. They possess excellent mechanical and tribological properties and are considered as potential engineering materials for various tribological applications [1]. Amongst a wide range of available matrix materials, zinc aluminum based alloys are most appropriate owing to their good bearing and wear properties, lower casting temperatures and lower cost [2]. Formation of zinc–aluminum (ZA) alloys containing a trace amount of copper have been observed to be possible cost and energy efficient substitutes for a variety of ferrous and non-ferrous alloys owing to their higher strength, better wear resistance, lower casting temperature and abundant resources [3]. ZA alloys are considered as prime bearing materials, especially suitable for high-load and low-speed applications [4]. Due to good tribo-mechanical properties such as low weight, excellent foundry casting ability, fluidity, good machining properties, hardness, corrosion resistance, low initial cost, energy-saving melting, environmental friendly technology and equivalent or even superior bearing and wear properties, ZA alloys (mostly ZA-12 and ZA-27) are capable of replacing aluminum cast alloys and bearing bronzes [4]. An important aspect that makes these alloys attractive is the reduction in cost from 25 to 50% and 40 to 75%, compared with aluminum and brass alloys respectively [5]. In recent years, reinforcing with a second phase particle (SPP) has been noted to substantially improve the mechanical

properties and wear response of zinc based materials. Various kinds of reinforcements like alumina [6–14], TiC [15], fly ash [16], zircon [17, 18], SiC [13, 19–22], mullite, i.e., aluminosilicate [10, 11], aluminite [23] in the form of particles [13, 15–23] and fibers [6–14] have been tried with an objective to realize property improvement of the alloy system. The effects of size [15], content [6–15, 17, 18, 23] and orientation of the reinforcement phase [8, 9] on mechanical and wear properties have also been earlier investigated. Hard and thermally stable ceramic reinforcements in zinc based alloys lead to less strength than the matrix alloy at ambient temperature [6, 14] although depending on the nature and type of the dispersoid phase, illustration of an opposite trend also exists [14]. Moreover, the composites attained improved and elevated temperature strength, increasing reinforcement content bringing about further improvement in the property. The dispersoid phase also caused higher hardness [6, 8, 10, 11, 13, 16–18], superior elastic modulus [6], greater dynamic modulus, better damping capacity [23] and less coefficient of thermal expansion [17] of the matrix alloy. As far as the utilization of a zinc based alloy/composite for abrasive wear application is concerned, only a few researchers have worked in this area [24–32]. In this context, few researchers [24, 25, 28, 30] reported that the SiC_p reinforcement improves the abrasive wear behavior of a zinc based alloy irrespective of the type of abrasive medium while similar observations were obtained with alumina particles dispersion [26, 27]. Moreover, the addition of nickel in appropriate amounts in zinc-aluminum alloys reduces the abrasion wear loss and the improvement in wear resistance increases with the amount of nickel [29]. Another study concluded that the abrasive wear resistance increases with a decrease in zinc concentration, also the abrasive size and zinc concentration have relatively less influence on the wear rate [31]. Recently three body abrasive wear properties of ZA-27 alloy were compared to CuSn10 bronze and it has been concluded that ZA-27 alloy exhibits better wear resistance than the CuSn10 bronze for high linear velocities [32].

It is to be noted that most of the available literature on zinc-based (particularly on ZA-27) composites are focused only on processing and their sliding wear behaviour, but no study converges on their abrasive wear characteristics. This leaves much scope for further investigation in the area. In view of the above, an attempt has been made in this study to analyze the abrasive wear behavior of ZA-27 alloys and its composite reinforced with 5 and 10 wt% SiC particles under the influence of varying applied loads and sliding distance. The influence of variation of SiC_p concentration in the matrix alloy towards controlling the wear behavior of the samples has been studied.

2 Experimental

2.1 Material Preparation

The zinc based matrix alloy and composites were prepared by a liquid metallurgy route using graphite crucibles for melting in an electric furnace. The composites were fabricated by incorporating 5 and 10 wt% of 50-80 μm silicon carbide particles on the vortex of the melt of the matrix alloy. The particles were preheated in the air at 600 °C for two hours prior to incorporation in the alloy melt. The vortex was created with a mechanical stirrer rotating at a speed of 600 rpm. Dispersion of the SiC particles in the melt was carried out at 700 °C while the pouring temperature was maintained at 750 °C. Permanent molds made of cast iron were used for the solidifying of the alloy and composites. The molds were also preheated to around 200 °C prior to pouring of the molten material. All the castings were made in the form of long cylindrical castings having 16 mm diameter and 170 mm length. Table 1 shows the chemical compositions of the test materials.

2.2 Microstructural Examination

Microstructural studies were carried out on 10 mm diameter, 15 mm thick samples. The samples were polished metallographically and etched suitably. Diluted aqua regia was used for etching the samples of the matrix alloy and composite. A microstructural characterization of the samples was carried out using scanning electron microscopy.

2.3 Quantitative Metallography

The SiC particles were dipped in alcohol and stirred for some time, and then with a pipette, a drop of alcohol plus particle slurry is placed on the double-sided tape fixed on a copper stud. After drying, the SiC particles on the copper stud were platinum coated and then observed by SEM in order to examine their morphology whereas size distribution of the particles was carried out using ImageJ [33].

Table 1 Chemical composition of the test material

Material	Elements, wt%				
	Zn	Al	Cu	Mg	SiC
Zinc-based alloy	Remaining	27.5	2.5	0.03	–
5% SiC composite	Remaining	27.5	2.5	0.03	5
10% SiC composite	Remaining	27.5	2.5	0.2	10

Similar measurements were also carried out on the abrasive particles bonded on the paper base.

2.4 Identification of Phases

X-Ray diffraction analysis of zinc-aluminum alloys their composites was carried out using a Rigaku (Model Miniflex-2) X-ray diffractometer to find out the phases present in the sample. The solid sample was packed on a sample holder of size 10 mm x 10 mm rectangular cavity having a depth of 2 mm. The samples were scanned at a scanning speed of 5 degrees (2θ) per minute in the diffraction angle (2θ) range of 32 to 47°, the measurement was done at an applied voltage of 30 kV and current of 15 mA. The X-ray diffractogram obtained from the test shows the relationship between diffraction angle (2θ) and relative intensity.

2.5 Measurement of Hardness and Density

The hardness of the test materials was measured on the Hv scale using a Vickers Hardness (Hv) testing machine (model: VM 50, FIE) according to ASTM standard E92-16 [34] describing the standard test method for a Vickers hardness of metallic materials. The specimen was polished metallographically and the opposite sides of the samples were made perfectly parallel before the hardness measurement. The Vickers hardness of the specimen was obtained at an applied load of 15 kg at a dwell time as 5 seconds from the indentation made using a square pyramidal diamond indenter having included face angles of 136°. Five hardness readings taken, and average values were reported. Density measurements were carried out using Archimedes principle. The samples required for density measurement were sectioned in a rectangular shape (15 x 15 x 10 mm). The sectioned samples were polished with 1200 grit polishing paper for all the surfaces of all the test materials. A Sartorius India Pvt. Ltd., Bangalore, India, (model CPA 2245) density kit was used for this purpose.

2.6 Abrasive Wear Test

High-stress abrasive wear tests were conducted on 30 mm long and 8 mm diameter cylindrical samples using a pin-on-disc equipment (Ducom, Bangalore, India, model TR-20M-106). The tests were conducted at room temperature as per ASTM G-132 standard [35]. Schematic representation of the pin-on-disc test assembly are shown in Fig. 1. The abrasive medium used in this study was a polishing/emery paper having SiC abrasive particles (18μm) firmly bonded on a strong paper base. The abrasive medium was firmly put in position on the disc of the machine. The samples were held against the rotating abrasive medium with the help of a specimen holder. Load on the sample was applied through a cantilever mechanism with the help of dead weights. The traversal distance, track radius load and the rotational speed of the disc was varied according to our need. The applied loads, in this case, were 1, 3, 5 and 7 N while the track diameters adopted were 10 cm which enabled the rotational speeds of 300 to attain linear sliding velocities of 1.57 m/s. The specimens were tested for 1.20, 2.40, 4 and 5.20 minutes to cover the distance 125, 250, 375 and 500 m respectively. The samples were polished metallographically, cleaned with acetone and weighed using the microbalance prior to testing. The tested samples were once again cleaned with acetone and weight loss taken at the continuous intervals. Friction force was measured using a load cell/force transducer placed to make contact with the rear end of the lever arm during the tests; the other end of the lever was connected with the sample in the holder. The friction force was read on a digital meter fixed with the control and display unit of the test set-up connected with the load cell. The measured friction force was then converted into the friction coefficient. The temperature at a distance of 1.5 mm from the contacting surface of the specimen was also monitored during the tests by inserting a chromel–alumel thermocouple in a 1.5 mm diameter hole made therein. An average of three observations was taken in this study.

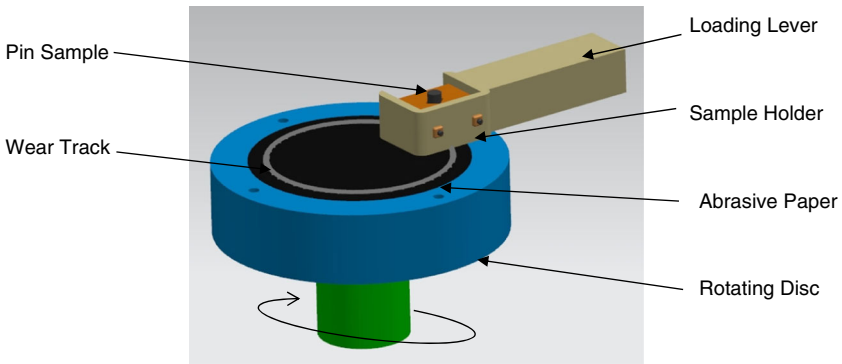

Fig. 1 Model of Pin-on-Disc Test Assembly

2.7 Wear Surfaces, Subsurface, Debris and Abrasive Medium Studies

Wear surface, subsurface regions, emery paper (fresh and tested) and debris were examined with a Carl Ziess model EVO-50 scanning electron microscope. Specimens tested at a minimum (1 N) and maximum (7 N) applied loads were considered for the SEM studies in the present investigation. The abraded surfaces were examined after ultrasonically cleaning the selected surfaces with acetone. For subsurface examination, typical specimens were sectioned perpendicularly to the abraded surfaces with a diamond cutter, mounted in polyester resin and polished metallographically and etched with diluted aqua regia before their examination in the SEM microscope to identify the microstructural changes in the subsurface, subsurface deformation and mechanically mixed layer. Fresh and tested emery papers under selected test conditions were mounted on brass studs using a double-sided carbon tape and examined under the SEM. Debris collected after the test was dispersed in acetone and spread on a glass slide. A brass stud covered with a double-sided carbon tape was used for mounting the debris for the SEM examination. Before conducting the scanning electron microscopic examination, the specimen were sputtered with gold.

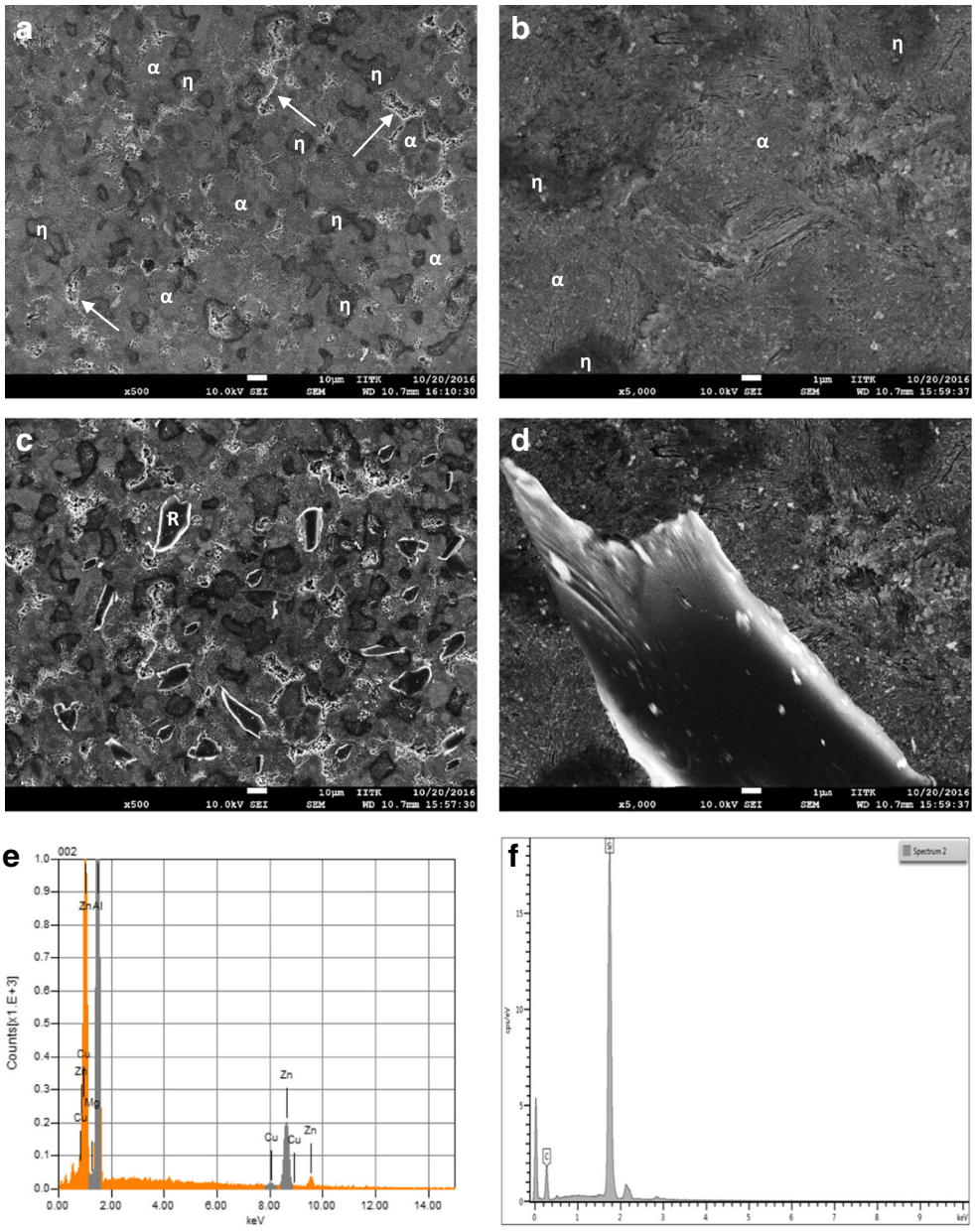

Fig. 2 Microstructure of ZA-27 Alloy (**a**, **b**) and ZA-27 + 10 % SiC Composite (**c**, **d**) {α-Al rich phase, η-Zn rich phase, arrow-ε: $CuZn_4$ metastable phase, R-reinforced SiC particles}

3 Results

3.1 Microstructure

Figure 2a–d represents the microstructure of the test materials. The base alloy exhibits a dendrite structure comprising of α-dendrites surrounded by $\alpha + \eta$ eutectoid and metastable ε phase in interdendritic regions as evidenced by EDXA shown in Fig. 2e. The composite showed similar features to those of the base alloy except the for additional presence of the reinforced SiC particles. A typical higher magnification micrograph (Fig. 2d) shows the interphase between SiC particles and the matrix alloy. Moreover, good interfacial bonding between the SiC particles and the metallic material and uniform distribution of SiC is also depicted in the figure. The EDXA analysis of the SiC-rich phase provides evidence for the presence of dispersed reinforcement particles in the matrix alloy (Fig. 2f).

3.2 Quantitative Metallography

A typical scanning electron micrograph of SiC particles shows the morphology of the particle (Fig. 3a). Note from the figure that the particles are equiaxed in nature, with sharp corners. The size distribution of silicon carbide particles is analyzed using an image analysis system. Particle size distribution is expressed in terms of accumulated wt% distribution and percentage frequency of particle size. The size range of silicon carbide particles was represented in the form of a histogram. Note from the figure that the maximum distribution of SiC particles ($\sim$ 34%) was obtained in the size range of 50-55 μm. The mode of distribution of the abrasive particles on the paper base is shown in Fig. 3b which clearly depicts the angular shape and sharp edges and corners of the abrasive particles. The size distribution of the abrasive particles on the paper base is also shown in Fig. 3b. The majority of the abrasive particles were observed to fall in the range of 16-20 μm ($\sim$ 70%).

3.3 XRD Analysis

The XRD patterns of the zinc based matrix alloy and 10% SiC reinforced composite are shown in Fig. 4. It was observed that there were four phases namely β, η (heavily zinc rich phase), α (aluminum rich phase) and ε (metastable $CuZn_4$ phase) present in the zinc based matrix alloys whereas in the case of composites along with the peaks of the matrix, SiC peaks were also present.

3.4 Hardness and Density

Figure 5 shows the density and hardness of the test materials. The addition of SiC increases the hardness but affects the density in the opposite manner. The matrix alloy has maximum density, followed by the ZA-27 Alloy + 5% SiC and the ZA-27 Alloy + 10% SiC reinforced composite. As far as hardness is concerned, the maximum is attained by the ZA-27 Alloy + 10% SiC and the minimum by the base alloy while the ZA-27 Alloy + 5% SiC composite showed an intermediate response.

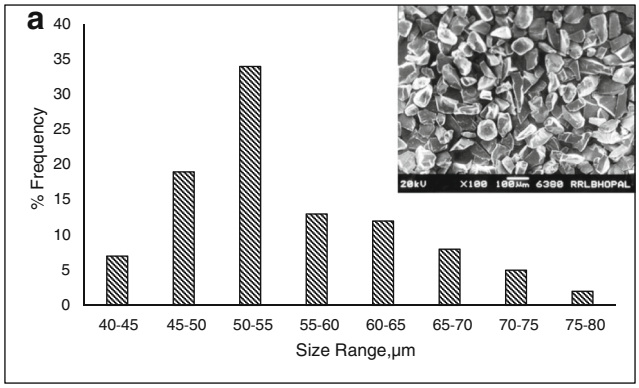

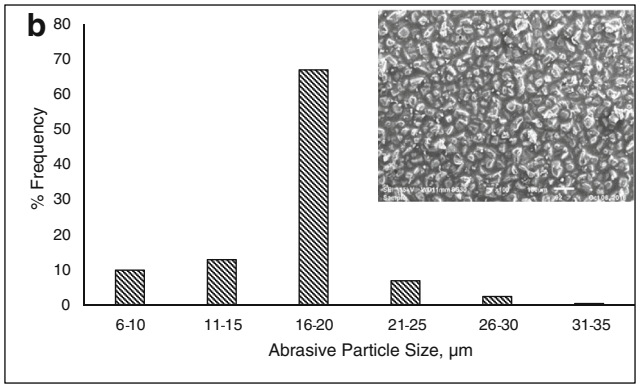

Fig. 3 Shape and size distribution of the reinforced SiC particles (**a**) and abrasive particles bonded to the paper base

3.5 Wear Behaviour

3.5.1 Wear Rate

Figure 6 delineates the wear rate of the test materials a function of abrading distance at an applied load of 1 N and 7 N. In general, the wear rate decreases with the increase in abrading distance for all the test materials and at both the loading conditions. It is also worth noting that the wear rate is maximum for the ZA-27 Alloy at 7 N and minimum for the ZA-27 + 10% SiC composite while the ZA-27 + 5% SiC composite revealed an intermediate response. Moreover, wear rate increases with the increase in applied load for all the test material, however, the slope of the increment is maximum for the base alloy followed by the 5% and 10% SiC composite (Fig. 7).

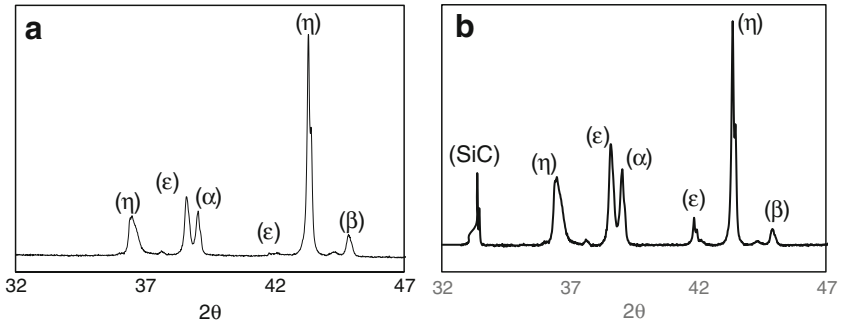

Fig. 4 XRD pattern of the zinc based matrix alloy (**a**) and 10% SiC reinforced composite (**b**)

3.5.2 Frictional Heating

Temperature near the contact surface for the ZA-27 Alloy, ZA-27 + 5% SiC and ZA-27 + 10% SiC composite at an applied load of 1 N and 7 N plotted as a function of abrading distance is shown in Fig. 8. The temperature rises linearly with the test duration and the maximum frictional heating is attained by the ZA-27 + 10% SiC composite followed by ZA-27 + 5% SiC and ZA-27 Alloy. As far as the effect of load on the frictional heating is concerned, the temperature increases with the increase in applied load irrespective of the test material, however, the severity of increase is maximum for the ZA-27 + 10% SiC composite and minimum for the ZA-27 Alloy (Fig. 9).

3.5.3 Friction Coefficient

Figure 10 represents the friction coefficient for the ZA-27 Alloy, ZA-27 + 5% SiC and ZA-27 + 10% SiC composite as a function of abrading distance at an applied load of 1 N and 7 N. The friction coefficient decreases with the increase in test duration for all the test materials and it is observed that the friction coefficient is maximum for the ZA-27 Alloy followed by the ZA-27 + 5% SiC and the ZA-27 + 10% SiC composite, however an increase in load increases the friction coefficient and the maximum increase is obtained for the ZA-27 Alloy and minimum for the ZA-27 + 10% SiC composite while the ZA-27 + 5% SiC composite revealed intermediate behaviour (Fig. 11).

3.5.4 Wear Surface

Figure 12 shows the abrasive wear surfaces of the matrix alloy tested at 1 N (a, b) and 7 N (c, d) load. In the case of low applied load fine abrasive grooves were generated. The grooves became deeper and wider at higher load. Sticking of debris, fragmented abrasive particles and fine pits were observed in the case of low load whereas in the case of high load microcracks and broad and deep grooves were observed.

Abraded surfaces of the 10% SiC reinforced composite tested at different applied loads are shown in Fig. 13. The intensity of the grooves on the surface increases with the increase in applied load. Although, in the case of low load, sticking of the abrasive in the microcracks is evident. In the case of high load, expulsion and fracturing of the reinforcement phase are evident. Moreover, the intensity of surface damage was less in the case of the composite as compared to the matrix alloy.

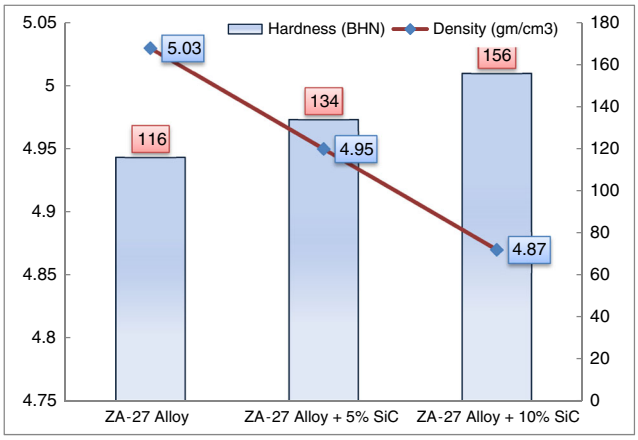

Fig. 5 Variation of hardness and density as a function of SiC content

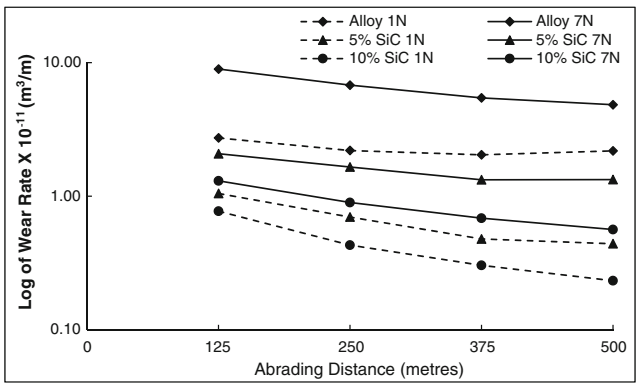

Fig. 6 Wear Rate of the samples plotted as a function of Abrading Distance at the applied load of 1 N and 7 N

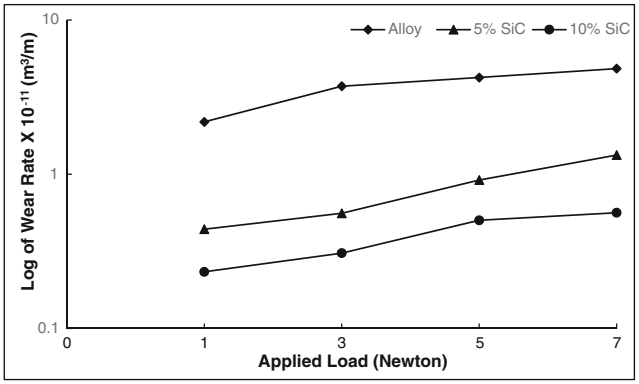

Fig. 7 Wear Rate of the samples plotted as a function of Applied Load

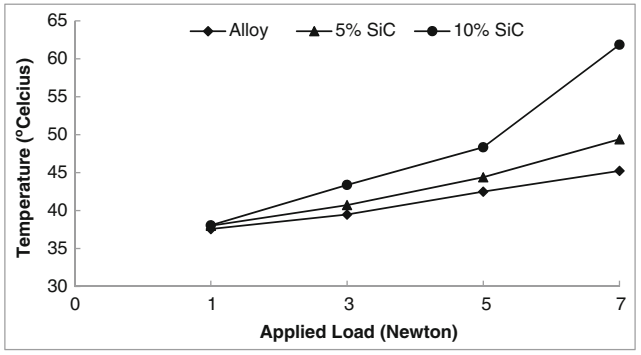

Fig. 9 Frictional heating of the samples plotted as a function of Applied Load

3.5.5 Wear Debris Analysis

Debris particles generated during the high-stress abrasion test of the matrix alloy under the action of 1 N and 7 N applied load is shown in Fig. 14. At the low load conditions small machining chips are generated while at higher load the majority of debris particles are long machining chips along with deformed flakes and a small amount of fragmented abrasive particles was observed. (regions marked by B and C respectively).

Figure 15 shows the debris particles of the 10% SiC reinforced composite under different loading conditions. The debris of the composite was similar to that of the matrix alloy except for the presence of a large quantity of fragmented abrasive particles. In the case of low load, fine debris particles were generated whereas in the case of higher load coarser debris was generated.

3.5.6 Examination of Degraded Abrasive Papers

Figure 16 shows the scanning electron micrographs of degraded abrasive paper after abrading the matrix alloy at an applied load of 1 N and 7 N. It was observed that the debris particles were deposited between the abrasive particles. The deposited debris particles are in the form of machining chips and deformed flakes. Moreover, the severity of deposition of the debris increases with the increase in applied load. However, at higher load, expulsion of abrasive particles from the paper base was also observed.

Degraded abrasive paper after abrading the 10% SiC reinforced composite at an applied load of 1 N (a, b) and 7 N (c, d) are depicted in Fig. 17. It is clear that microcracking, fracturing, and partial removal of the abrasive particles are the common phenomena. At lower load sticking of the fine debris is observed while in the case of higher load the protruding action of the abrasive particles is reduced.

3.5.7 Subsurface Examination

Figure 18 shows the scanning electron microscopic views of subsurface features of the matrix alloy and the 10% SiC composite at an applied load of (a, b) 1 N and (c, d) 7 N respectively for 500 meters abrading distance. The changes involved plastic deformation, breaking of the microconstitutents and subsurface cracking. The presence of SiC particles in the matrix significantly reduced the extent of plastic

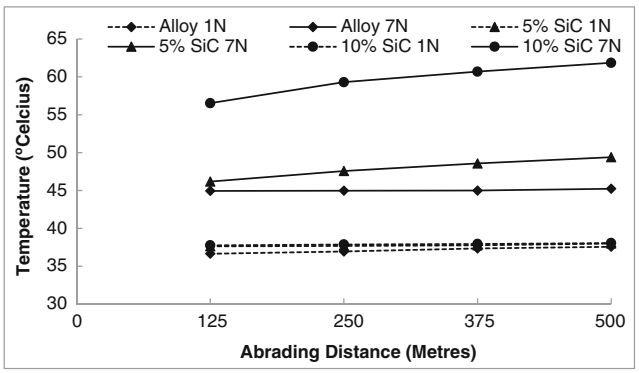

Fig. 8 Frictional Heating of the samples plotted as a function of Abrading Distance at the applied load of 1 N and 7 N

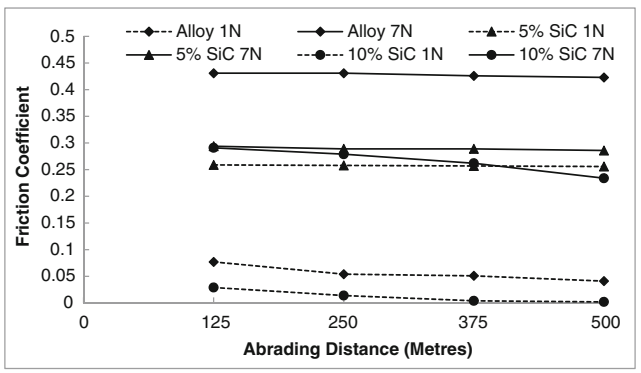

Fig. 10 Friction Coefficient of the samples plotted as a function of Abrading Distance at the applied load of 1 N and 7 N

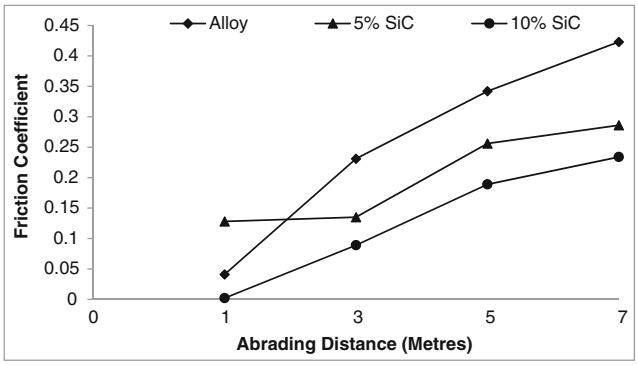

Fig. 11 Friction Coefficient of the samples plotted as a function of Applied Load

deformation and the thickness of the deformed region. However, decohesion of the dispersoid phase at the interfacial regions along with the microcracking of the dispersoid phase is evident in this case.

4 Discussion

The major alloying element in zinc based alloys is aluminum which controls the solidification behavior and the microstructure. It has been reported that addition of aluminum to zinc imparts fluidity and refines the grain size. The microstructure of zinc aluminum alloys consists of a mixture of α-Al (Al-rich solid solution) and η (zinc-rich solid solution) phases at room temperature distributed in a specific manner depending on the concentration of Al present therein [36]. The ε ($CuZn_4$) intermetallic phase has been reported to participate out in the interdenditic channels of Zn-Al alloys containing copper beyond 1% [37]. Magnesium (0.01-0.05%) present in the Zn-Al alloys remains dissolved in the solid solution of the alloy [36, 38]. Based on the binary Zn-Al equilibrium diagram [36, 38], ZA-27 alloy containing 27.5% aluminum falls in the hypereutectoid range. Therefore the microstructure of the alloy is primary α-dendrites surrounded by the $\alpha + \eta$ eutectoid as well as the metastable ε-phase.

The incorporation of SiC in the zinc based matrix alloys has a significant effect on the size of dendrites in the matrix alloy. The microstructure of SiC reinforced composites is mainly made up of equiaxed grains. During solidification, most SiC particles are supposed to act as nucleation sites for the primary phase in the matrix alloy. The dispersed SiC particles are considerably harder than the base alloy and enhance the abrasion resistance of the matrix alloy.

The morphology of the silicon carbide reinforcement is understood through SEM micrographs (Fig. 3a) which clearly depict the sharp edged equiaxed morphology. As noted from the literature, the type, shape and size of the reinforcement directly affect the properties of the composites [39]. Hence, it was found necessary to understand the basic structure of the reinforcements. The morphology of abrasive grit papers indicating SiC abrasives is shown in Fig. 3b. It is observed that grits on the emery papers are arranged in a discontinuous fashion and are not aligned or oriented in one particular direction.

The XRD patterns of the matrix materials and 10% SiC composite are shown in Fig. 4. The main phases identified

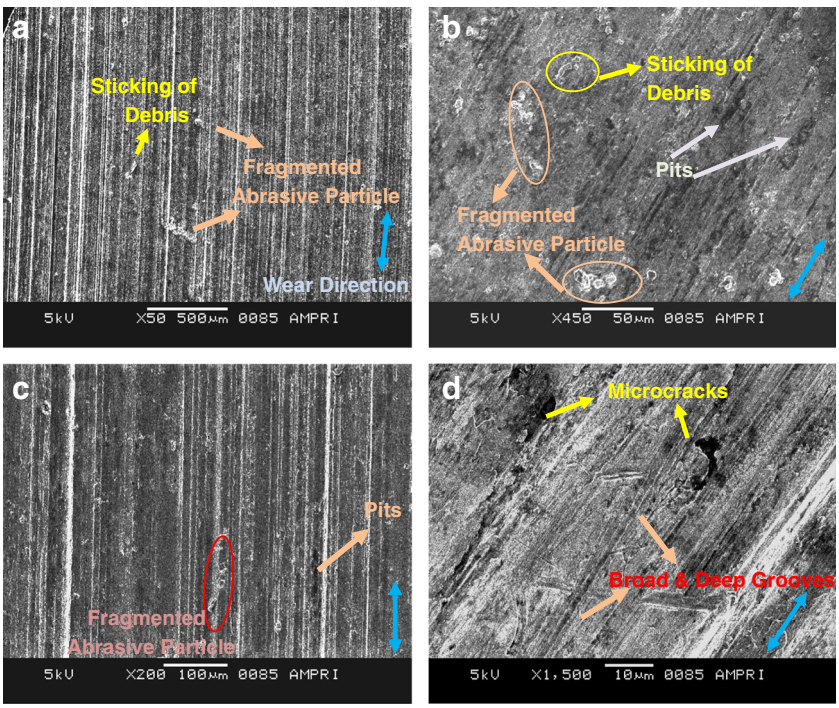

Fig. 12 Wear surfaces of the zinc based matrix alloys tested at an applied load of 1 N (**a**, **b**) and 7 N (**c**, **d**)

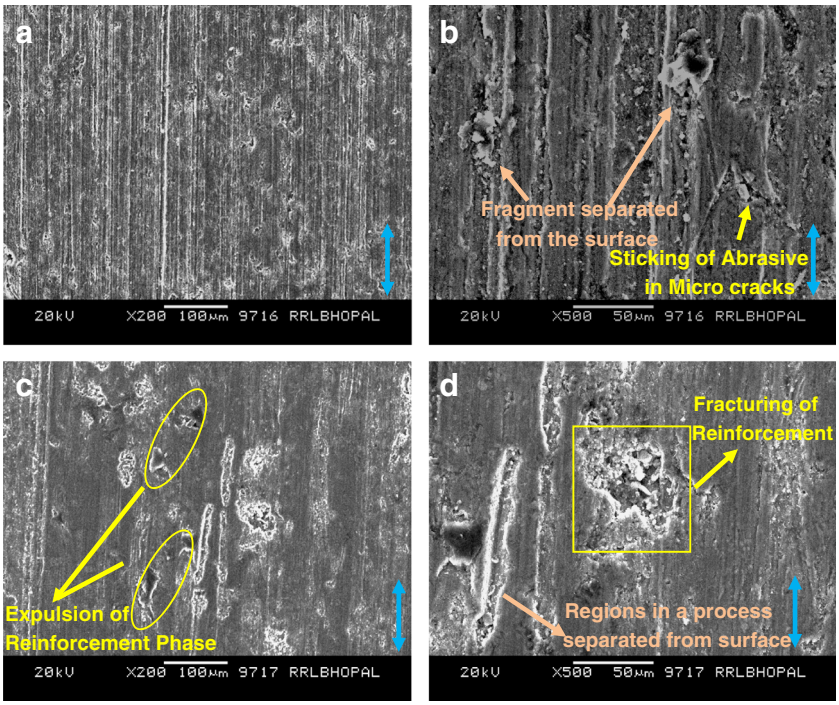

Fig. 13 Wear surfaces of the 10% SiC reinforced composite tested at an applied load of 1 N (**a**, **b**) and 7 N (**c**, **d**)

in the matrix alloys are α(Al), η(Zn) and ε($CuZn_4$) while in the case of composites additional SiC peaks are present along with the peaks of the matrix alloys. The presence of SiC peaks in the composites confirms the dispersion of SiC particles within the melt. α and η are Al and Zn rich solid solutions having crystal structures as FCC and HCP respectively [40]. The intermediate product ε is a metastable $CuZn_4$ phase form when the alloy system contains Cu above

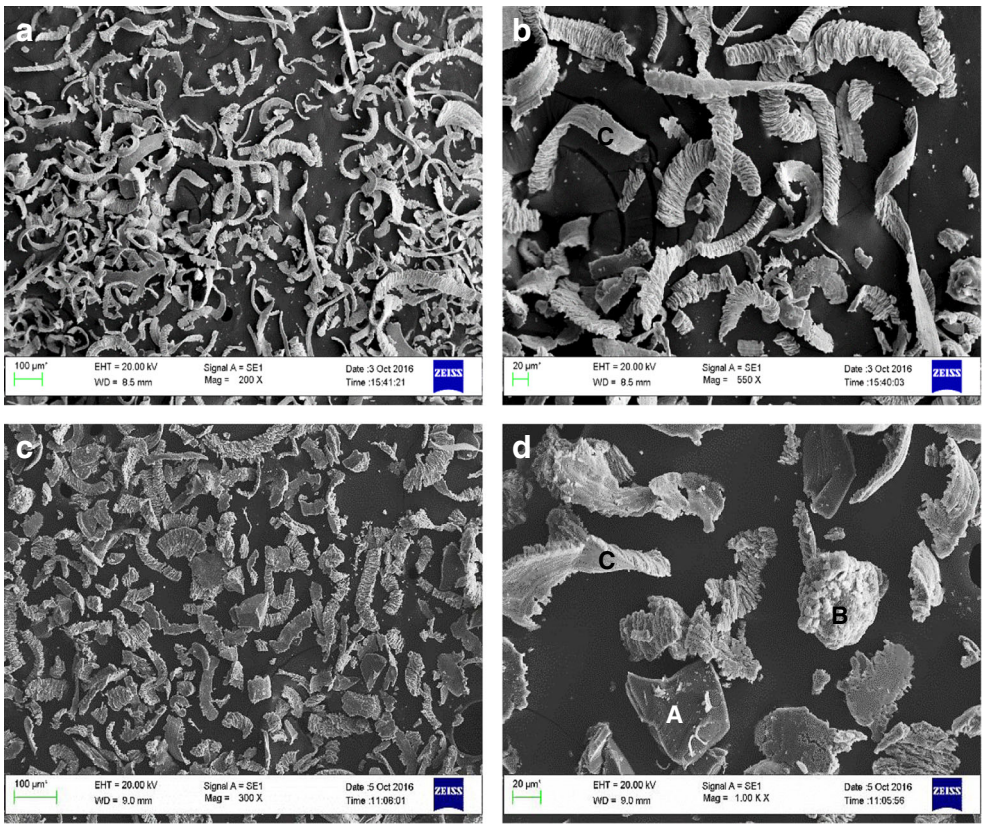

Fig. 14 Wear debris of the matrix alloy tested at the applied load of 1 N (**a**, **b**) and 7 N (**c**, **d**){A: fragmented abrasive/reinforcement particle, B: deformed flake, C: machining chips}

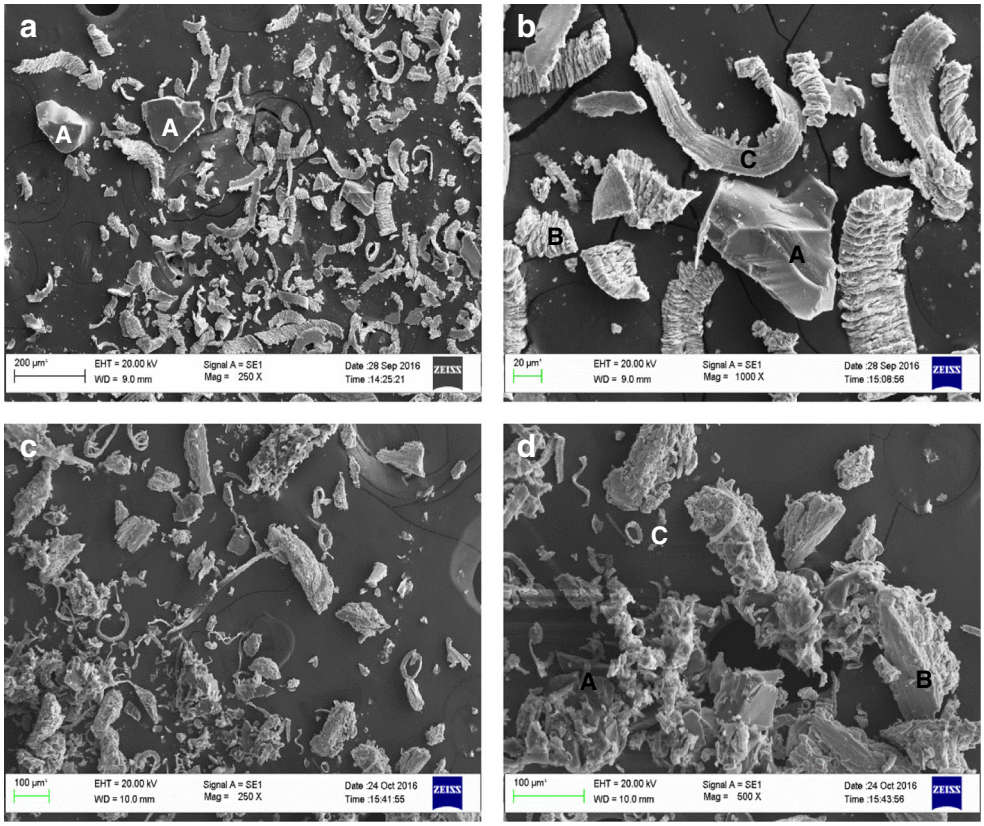

Fig. 15 Wear debris of the 10% SiC composite tested at the applied load of 1 N (**a**, **b**) and 7 N (**c**, **d**){A: fragmented abrasive/reinforcement particle, B: deformed flake, C: machining chips}

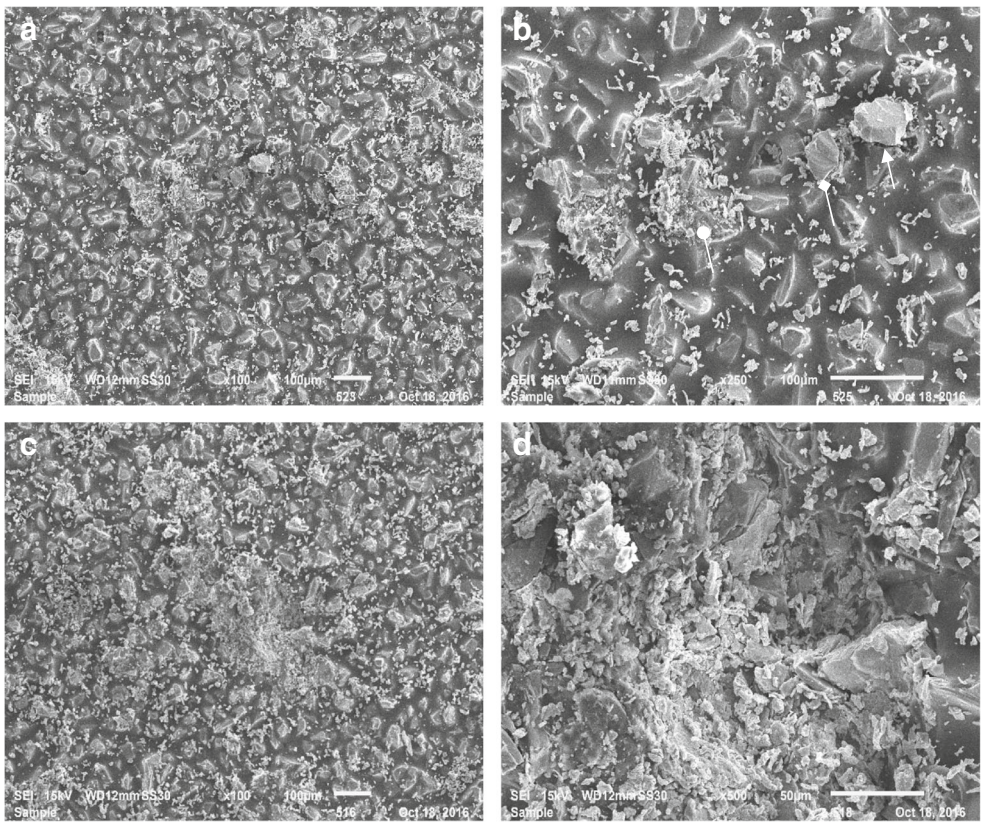

Fig. 16 Abrasive grit paper after abrading the zinc based matrix alloy at 1 N (**a**, **b**) and 7 N (**c**, **d**) load {*Arrow*: microcracking, *diamond arrow*: protruded abrasive particle, *oval arrow*: fracturing of abrasive particle}

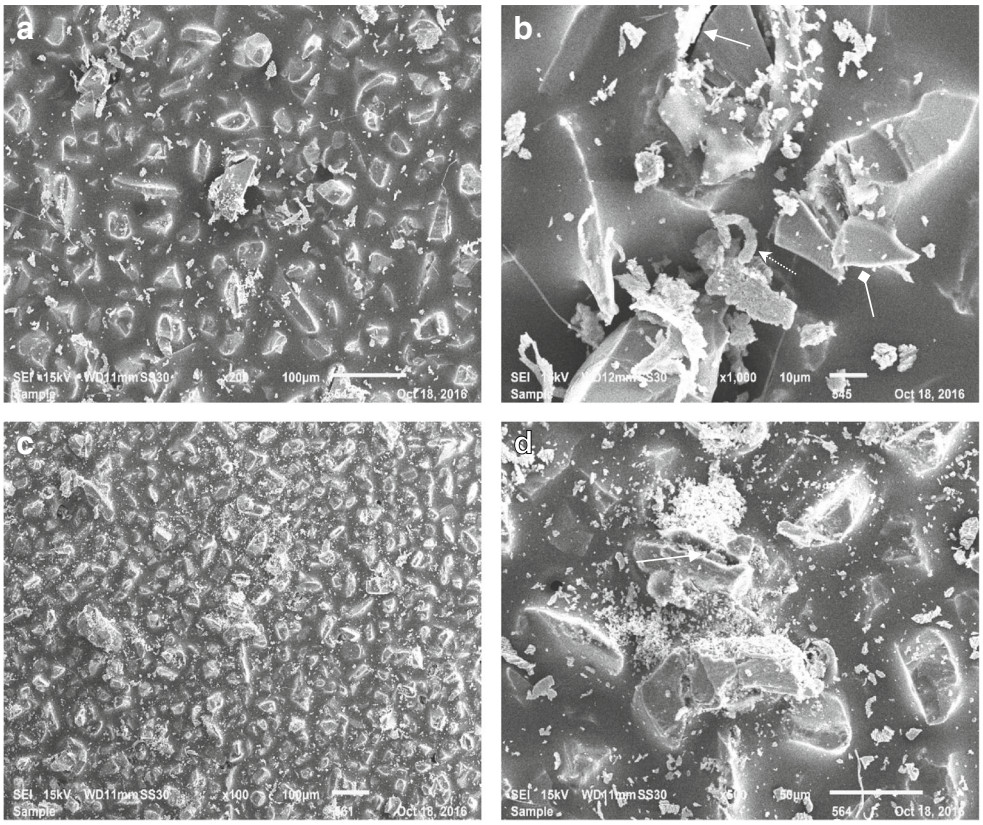

Fig. 17 Abrasive grit paper after abrading 10% SiC Composite at 1 N (**a**, **b**) and 7 N (**c**, **d**) load {*Arrow*: microcracking, *diamond arrow*: protruded abrasive particle, *oval arrow*: fracturing of abrasive particle, *dotted arrow*: deposited debris particles}

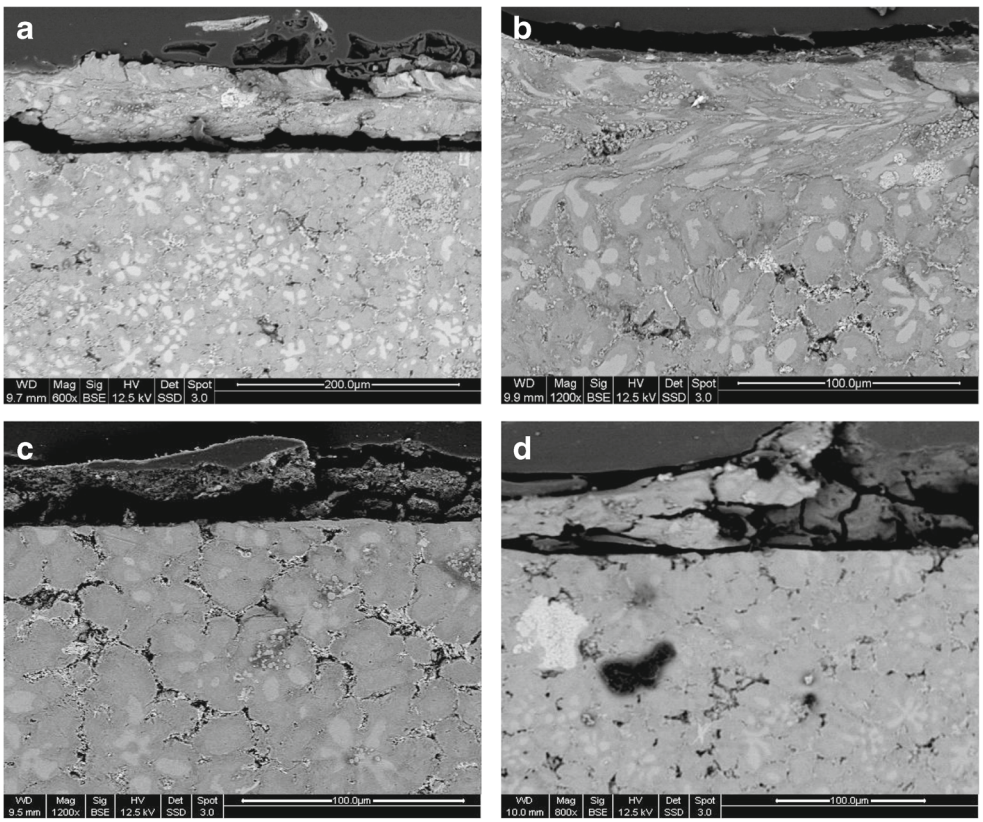

Fig. 18 Subsurface Regions of a Matrix alloy (**a**, **b**) and 10% SiC Composite (**c**, **d**) tested at 1 N (**a**, **c**) and 7 N (**b**, **d**) load

1%. In the present study, the alloy selected contained 2.5% Cu leading to the formation of the ε phase. It is also noticed from the XRD analysis that Al_2O_3, ZnO and other undesirable compounds are not detected in the composites, it is thus claimed that the present method is a feasible technique to fabricate zinc based composites.

It is revealed from Fig. 5 that the specimens show an increase in hardness as the content of SiC in the composite is increased. As is known, hardness measures resistance to indentation wherein there will be localized plastic deformation under standardized conditions. The increase in hardness is obvious and expected since SiC particles being hard dispersoids contribute positively to the hardness of the composites. The increased hardness is attributed to the hard SiC particles which act as barriers to the movement of dislocations within the matrix. This dispersion-strengthening effect is expected to be retained even at elevated temperatures and for extended time periods because the particles are not reactive with the matrix phase.

The abrasive wear is associated with the penetration of the hard rigid abrasives and subsequent scratching of the specimen surface by the penetrated abrasives. The scratching of the abrasives leads to the continuous groove marks. The depth of penetration (i.e., the width and the depth of grooves) depends on applied load and relative hardness of the abrasive with respect to the specimen surface hardness. As the hardness of the composite is higher than that of the alloy, it is expected that the depth of penetration of the abrasive in the composite surface is less as compared to the alloy. Additionally, SiC particles on the composite surface act as protrusions, which carry the major portion of the applied load and this helps in protecting the matrix alloy from severe contact of abrasives. As a result, relatively less material is removed from the composite surface as compared to the alloy due to a cutting or plowing action. The wear resistance of the composite also depends to a significant extent on the interfacial bonding between SiC and the matrix alloy and the fracturing tendency of SiC particles. It is reported by several earlier studies that the composite is superior to the alloy (as far as wear resistance is concerned) provided the bonding is strong enough to hold the particle on the wear surface intact and the hard ceramic particles are not fractured or fragmented. Important events during abrasion of the samples as far as the abrasive particles are concerned include capping, clogging, shelling and attrition. Especially attrition becomes quite effective in reducing the abrasion rate when the same abrasive comes in contact with the specimen surface in a cyclic manner [24, 39]. Interaction with relatively sharper abrasive particles in the starting of the tests could lead to a higher rate of increase in wear rate and temperature. As the test duration increases to sufficiently dull the abrasive particles, the rate of increase is reduced.

Highest friction coefficient and frictional heating of the most ductile (zinc-based) matrix alloy could be due to a larger depth of penetration of the abrasive particles in the samples. A reduction in the severity of penetration due to the hard SiC reinforcement in the alloy matrix causes the friction coefficient and frictional heating of the composite to decrease on the contrary to that of the matrix alloy. Higher wear rate, friction coefficient and frictional heating with increasing load may be attributed to a larger depth of penetration by the abrasive particles on the specimen surface [24, 39]. The friction coefficient in turn appears to have predominantly been controlled by the factors like capping, clogging, shelling and attrition of the abrasive particles leading to a decrease in their cutting efficiency/depth of penetration [24, 28, 39] and hence a reduction in the friction coefficient of the samples with test duration.

5 Conclusion

The matrix alloy exhibits dendrite structure comprising α-dendrites surrounded by the $\alpha + \eta$ eutectoid and the metastable ε phase in the interdendritic regions. The composite shows similar behavior to that of the base alloy except for the additional presence of the reinforcing SiC particles.

Incorporation of SiC particles reduces the density but increases the hardness of the base alloy.

The wear rate decreases with the increase in abrading distance for all the test materials and at all the loading conditions. Dispersion of SiC particles reduces the wear rate. The increment in the applied load increases the wear for all the test materials however, the slope of the increase is maximum for the base alloy followed by 5% and 10% SiC.

The temperature rises linearly with the test duration and the ZA-27 + 10% SiC composite attained maximum frictional heating followed by the ZA-27 + 5% SiC and the ZA-27 alloy. The increase in applied load increases the temperature irrespective of the test material however the severity of increase is maximum for the ZA-27 + 10% SiC composite and minimum for the ZA-27 Alloy.

The friction coefficient decreases with the increase in test duration for all the test materials and maximum friction coefficient is observed for the ZA-27 Alloy followed by the ZA-27 + 5% SiC and the ZA-27 + 10% SiC composite. Increases in load increase the friction coefficient and the maximum increase is obtained for the ZA-27 Alloy and is minimum for the ZA-27 + 10% SiC composite while the ZA-27 + 5% SiC composite showed intermediate behaviour.

High wear rate can be evinced by large damage to the pin surface, coarse debris formation and less damage to the abrasive particles whereas the opposite trend was observed in the case of low wear rate.

References

1. Kumar MP, Sadashivappa K, Prabhukumar GP, Basavarajappa S (2006) Dry sliding wear behaviour of garnet particles reinforced zinc-aluminium alloy metal matrix composites. Mater Sci-Medziagotyra 12(3):1392–1420
2. Tjong SC, Chen F (1997) Wear behavior of as-cast ZnAl27/SiC particulate metal-matrix composites under lubricated sliding condition. Metall Mater Trans A 28a:1951–1955
3. Chen T, Yuan C, Fu M, Ma Y, Li Y, Hao Y (2009) Friction and wear properties of casting in-situ silicon particle reinforced ZA27 composites. Chin Foundry 6(1):1–8
4. Babic M, Slobodan M, Dzunic D, Jeremic B, Ilija B (2010) Tribological behavior of composites based on ZA-27 alloy reinforced with graphite particles. Tribol Lett 37:401–410
5. Dominguez C, Moreno-lopez MV, Rios-jara D (2002) The influence of manganese on the microstructure and the strength of a ZA-27 alloy. J Mater Sci 37:5123–5127
6. Zhu HX, Liu SK (1993) Mechanical properties of squeeze-cast zinc alloy matrix composites containing α-alumina fibres. Composites 24.5:437–442
7. Dahotre NB, Dwayne McCay T, McCay MH (1990) Laser surface modification of zinc-base composites. JOM 42.6:44–47
8. Sahin Y (1998) Wear behaviour of planar-random fibre-reinforced metal matrix composites. Wear 223.1:173–183
9. Yu S, He Z, Chen K (1996) Dry sliding friction and wear behaviour of short fibre reinforced zinc-based alloy composites. Wear 198.1:108–114
10. Muthukumarasamy S, Guruprasad A, Sudhakar A, Seshan S (1996) Moore proceedings of the conference on process. Fabri. Adv. Mater. In: Sudarshan TS, Moore JJ (eds) The minerals. Metals and Materials Society, pp 111-125
11. Muthukumarasamy S, Seshan S (1995) Structure and properties of fibre reinforced zn-27% al alloy based cast MMCs. Composites 26.5:387–393
12. Genel K, Kurnaz SC, Durman M (2003) Modeling of tribological properties of alumina fiber reinforced zinc–aluminum composites using artificial neural network. Mater Eng A 363.1:203–210
13. Cornie JA, Guerriero R, Meregalli L, Tangerini I (1988) Proceedings of the conference on cast reinforced metal composites, Chicago, Illinois. USA. ASM Int, Metals Park, pp 155–165
14. Lo SHJ et al (1992) Mechanical and tribological properties of zinc-aluminium metal-matrix composites. J Mater Sci 27.21:5681–5691
15. Ylmaz O, Turhan H (2002) Wear behaviour of ZnAl27/TiCp metal matrix composites under sliding conditions. Mater Sci Technol 18.4:401–406
16. Koti MS (2000) Proceedings of the third international conference on Adv Compo. (ADCOMP-2000). FAME Bangalore, Bangalore, pp 717–723
17. Li BJ, Chao CG (1996) Mechanical properties and 95° aging characteristics of zircon-reinforced Zn-4Al-3Cu alloy. Metallur Mater Trans A 27.3:809–818
18. Sharma SC, Girish BM, Somashekar DR, Satish BM, Kamath R (1999) Sliding wear behaviour of zircon particles reinforced ZA-27 alloy composite materials. Wear 224(1):89–94
19. Prasad BK, Das S, Modi OP, Jha AK, Dasgupta R, Yegneswaran AH (1999) Wear response of a Zn-base alloy in the presence of SiC particle reinforcement: a comparative study with a copper-base alloy. J Mater Eng Perform 8(6):693–700
20. Prasad BK, Jha AK, Das S, Modi OP, Dasgupta R, Yegneswaram AH (1999) Sliding wear response of a Zinc Aluminium alloy as affected by SiC particle dispersion and test condition. J Mater Sci Lett 18:1731–1734
21. Sharma SC, Girish BM, Kamath R, Satish BM (1997) Effect of SiC particle reinforcement on the unlubricated sliding wear behaviour of ZA-27 alloy composites. Wear 213(1):33–40
22. Prasad BK (2003) Influence of some material and experimental parameters on the sliding wear behaviour of a zinc-based alloy, its composite and a bronze. Wear 254.1:35–46
23. Sastry S, Krishna M, Uchill J (2000) Proceedings of the third international conference on adv. compo. (ADCOMP-2000). FAME Bangalore, Bangalore, pp 510–516
24. Prasad BK, Das S, Jha AK, Modi O, Dasgupta R, Yegneswaran AH (1997) Factors controlling the abrasive wear response of a zinc-based alloy silicon carbide particle composite. Compos Part A 28A:301–308
25. Prasad BK, Das S, Dasgupta R, Modi O, Jha AK, Yegneswaran AH (1998) Two-body abrasion characteristics of a zinc-based alloy: effects of SiC particle reinforcement and related factors. J Mater Sci Lett 17:901–903
26. Modi O, Yadav R, Mondal D, Dasgupta R, Das S, Yegneswaran AH (2001) Abrasive wear behaviour of zinc-aluminium alloy - 10% Al_2O_3 composite through factorial design of experiment. J Mater Sci 36:1601–1607
27. Modi O, Yadav R, Prasad B, Jha A, Das S, Yegneswaran AH (2001) Three-body abrasion of a cast zinc–aluminium alloy: influence of Al_2O_3 dispersoid and abrasive medium. Wear 249:792–799
28. Prasad B (2002) Abrasive wear characteristics of a zinc-based alloy and zinc-alloy/SiC composite. Wear 252:250–263
29. Choudhury P, Das S, Datta B (2002) Effect of Ni on the wear behavior of a zinc-aluminum alloy. J Mater Sci 37:2103–2107
30. Prasad B, Modi O, Khaira H (2004) High-stress abrasive wear behaviour of a zinc-based alloy and its composite compared with a cast iron under varying track radius and load conditions. Mater Sci Eng A 381:343–354
31. Mondal D, Das S, Rajput V (2005) Effect of zinc concentration and experimental parameters on high stress abrasive wear behaviour of Al–Zn alloys: a factorial design approach. Mater Sci Eng A 406:24–33
32. Hamdullah C, Serdar CH (2011) Investigation of the abrasive wear behaviour of ZA-27 alloy and CuSn10 bronze. J Mater Sci 46:4850–4857
33. Rasband WS (2014) ImageJ 2014
34. ASTM E92–16, Standard Test Methods for Vickers Hardness and Knoop Hardness of Metallic Materials
35. ASTM G132 – 96 (Reapproved 2013) Standard Test Method for Pin Abrasion Testing
36. Apelian D, Paliwal M, Herrschaft DC (1981) Casting with zinc alloys. Jom 33.11:12–20
37. Gervais E, Barnhurst RJ, Loong CA (1985) An analysis of selected properties of ZA alloys. JOM 37.11:43–47
38. Lodder LAJ (1954) Non-ferrous foundry metallurgy. In: Murphy AJ (ed). McGraw Hill, New York, p 445
39. Prasad BK, Jha AK, Modi O, Das S, Yegneswaran AH (1995) Abrasive wear characteristics of Zn-37.2 Al-2.5Cu-0.2Mg alloy dispersed with silicon carbide particles. Mater Trans JIM 36(8):1048–1057
40. Engineering Properties of Zinc Alloys International Lead Zinc Research Organization, Inc. Third Edition August (1988)